Thermal Conductivity of n-Type Germanium from 0.3 to 4.2 K*

Bruce L. Bird† and Norman Pearlman
Department of Physics, Purdue University, Lafayette, Indiana
(Received 20 April 1971)

The thermal conductivity of lightly Sb-, P-, and As-doped germanium was measured between 0.3 and 4.2 K. The strong scattering of phonons by neutral donors observed earlier above 1 K diminishes below 1 K, as predicted by the theories of Keyes and of Griffin and Carruthers. Inclusion of resonance fluorescence of phonons, as proposed by Griffin and Carruthers, improves agreement with the measured thermal conductivity (except at the lowest temperatures, where neither their theory nor that of Keyes fits the data very well) and leads to the value 16 eV for the deformation potential and to simple-hydrogenic-model values for the effective radii of the donor ground states. The divergence of the data from the calculated values at the lowest temperatures is evidence for an additional scattering mechanism effective below 1 K, possibly associated with phonon-assisted hopping between donor atoms.

I. INTRODUCTION

This paper describes measurements made on the thermal conductivity of germanium doped with either antimony (Sb), arsenic (As), or phosphorus (P) in the temperature range from 0.3 to 4.2 K and with impurity concentrations from 3×10^{14} to 3×10^{16} atoms per cm^3. The experimental results are compared with previously proposed theoretical calculations based on a model of phonon scattering due to the electron bound to the added impurity atom.[1,2]

The temperature dependence of the thermal conductivity reflects the frequency and temperature dependence of various phonon-scattering processes occurring in the solid. In the single relaxation-time approximation the collision operator $(\partial N/\partial t)_{\text{coll}}$, which appears in the Boltzmann transport equation and represents the combined effect of all phonon-scattering processes occurring in the solid, is assumed to be $(\partial N/\partial t)_{\text{coll}} = -(N-N_0)/\tau$, where N_0 is the equilibrium phonon distribution, N is the phonon distribution at time t, and τ is the total relaxation time of the phonon distribution. τ is usually calculated by setting $\tau^{-1}=\sum_i \tau_i^{-1}$, where the τ_i^{-1} are the relaxation times for separate phonon-scattering processes due to boundaries, point defects, isotopes, other phonons, etc. By adjusting the strength of the different scattering processes, a reasonably good fit can be made to the thermal conductivity of pure insulators and semiconductors from 1 to 300 K.

If a particular type of defect is added to the pure crystal, then any changes occurring in the measured thermal conductivity can be compared with theoretical calculations using a total relaxation time $\tau^{-1} = \tau_D^{-1} + \tau_P^{-1}$, where τ_D^{-1} is the phonon-scattering probability due to the added defect and $\tau_P^{-1}=\sum_i \tau_i^{-1}$ represents the phonon-scattering processes occurring in the "pure" crystal (see Appendix A). This comparison then suggests whether or not the model of the defect to obtain τ_D is reasonable and, hopefully, enables some parameters of the defect to be determined.

Electrically active impurity atoms in semiconductors provide an attractive defect to be studied by thermal-conductivity measurements because of the purity and structural perfection of the host lattice and the ease with which definite amounts of a known impurity can be added over a wide range of concentrations. Several review articles[3-5] have appeared recently describing thermal-conductivity measurements on both doped and undoped Ge, Si, III-V compounds, and II-VI compounds.

Previous measurements of the low-temperature thermal conductivity of both n-type germanium[6-8] [containing from 10^{15} to 10^{18} group-V (Sb, As, or P) impurity atoms per cm^3] and p-type germanium[9,10] [containing from 10^{14} to 10^{19} group-III (In, Ga) impurity atoms per cm^3] have shown that shallow donors or acceptors in germanium are very strong scatterers of phonons. (See Appendix B for a brief summary of the properties of these states which are relevant to our measurements.) For example, a concentration of as little as 4×10^{16} Sb donors per cm^3 reduces the thermal conductivity at 2 K by a factor of 8.

Goff and Pearlman[6,7] compared measurements made on highly doped highly compensated n-type samples with those made on singly doped samples with the same concentration of neutral donors. They found that the extra thermal resistance introduced by the impurity was correlated with the number of neutral donors and not with the total impurity concentration. Thus the phonon scattering occurs because of an interaction with the electron bound to the donor ion, not with the donor ion itself. An impurity species effect was also found; Sb is a more effective scatterer of phonons than either As or P for concentrations less than 6×10^{17} cm^{-3}. For higher concentrations, where the donor levels have merged with the conduction band, the extra thermal resis-

tance is species independent.

We can thus recognize two distinct phonon-scattering processes; one for low concentrations where the electron is bound to the donor impurity, and the other for high concentrations where the electron is free to move in the conduction band. In this article we will only consider the case of low-concentration noncompensated samples for which the donor electrons are assumed to be isolated. Such material most nearly conforms to the assumptions used in the models of Keyes[1] and of Griffin and Carruthers[2] (expressions for the inverse relaxation time τ_{ep}^{-1} calculated from these models are given in Appendix C). Both treatments predicted a large decrease in τ_{ep}^{-1} at sufficiently low temperature, but the earlier measurements down to about 1 K gave no sign of the corresponding increase in K. By extending the measurements below 1 K we were able to observe the expected increase in K, but at the same time we found evidence for another phonon-scattering mechanism which apparently had not been observed before.

II. APPARATUS AND SAMPLES

A. Apparatus

The measurements were made in a recirculating He^3 cryostat[11] capable of covering the range from 0.27 and 4.2 K. The thermal conductivity was measured using the absolute method with the temperature difference along the samples determined by two germanium resistance thermometers. These thermometers were $0.5\times1\times3$-mm bars cut from germanium which had been highly doped with antimony and then highly compensated with gallium. The resulting material is n type with a room-temperature resistivity of approximately 0.06 Ω cm. The germanium thermometers were calibrated each run against the vapor pressures of He^3 and He^4 from 0.7 to 4.2 K using Montgomery's[12] polynomial expansions relating the absolute temperature to the vapor pressure of He^3 or He^4.

Below 0.7 K the calibration temperatures were determined by a magnetic thermometer consisting of a set of mutual inductance coils and a spherical sample of powdered compressed chromic methylammonium alum (CMA). The mutual inductance M of the magnetic thermometer varies with temperature as $M=A+B/T^*$, where the magnetic temperature T^* for this salt is related to the absolute temperature $T^*=T+0.00279/T+10.5\times10^{-3}$ down to at least 0.5 K according to Roberts *et al.*[13] The constants A and B were determined by calibrating the magnetic thermometer above 0.7 K against the vapor pressures of He^3 and He^4.

A least-mean-square fit of the calibration data of each thermometer was then made to an expansion of $1/T$ in powers of $\log_{10}R$, i.e.,

$$1/T=A_0+A_1\log_{10}R+A_2(\log_{10}R)^2+A_3(\log_{10}R)^3\ , \quad (1)$$

as suggested by Moody and Rhodes.[14] The temperature range from 0.27 to 4.2 K, containing approximately 26 calibration points, was divided into three overlapping intervals and the A_i's were determined for each interval. Agreement between the temperatures calculated from the above expression and the actual calibration temperatures is within 2 mK for temperatures greater than 2.2 K and within 1 mK for temperatures less than 2.2 K.

B. Description of Samples

When first cut from the ingot with a diamond saw, the samples were rectangular prisms with approximate dimensions of $5\times5\times25$ mm. The long axis of the sample is in the [100] direction which is perpendicular to the growth axis of the crystal in order to minimize any impurity concentration gradients. Before mounting the samples, all surfaces were ground with No. 280 carborundum powder. This reduces the sample dimension to approximately $4\times4\times24$ mm and produces a diffuse boundary scattering surface. The cross-sectional area A of the samples is listed in Table I.

The impurity concentrations of the samples were determined from the room-temperature Hall coefficient R using the expression

$$n=-rS/eR, \quad (2)$$

where n is the concentration of electrons in the conduction band at room temperature, e is the charge of the electrons, S depends upon the shape of the band involved (for germanium $S=0.784$),[15] and $r=\mu_H/\mu$ is the ratio of the Hall mobility to the electrical conductivity mobility ($r=1.18$ assuming pure-lattice scattering).[16]

Germanium at room temperature is in the exhaustion range, that is, all donors are ionized so that $n=n_{ex}=N_D-N_D\cong N_D$, where N_D is the donor concentration, N_A is the acceptor concentration, and n_{ex} is the number of electrons bound to donor atoms at low temperatures. For uncompensated n-type germanium, and acceptor concentration N_A of from 3 to 6% of the donor concentration is usually found.[17] Values of n_{ex} listed in Table I are

TABLE I. Sample parameters.

Sample	n_{ex} (cm^{-3})	A (cm^2)	L_c (cm)
Ge-543	5.4×10^{13}	0.154	0.443
Sb-344	3.4×10^{14}	0.151	0.438
Sb-365	3.6×10^{15}	0.171	0.468
Sb-306	3.0×10^{16}	0.162	0.455
P-375	3.7×10^{15}	0.162	0.455
P-266	2.6×10^{16}	0.165	0.459
As-276	2.7×10^{16}	0.144	0.428

probably accurate to within 10%.

III. THERMAL-CONDUCTIVITY MEASUREMENTS AND COMPARISON WITH THEORY

The measured thermal conductivity of the various samples is plotted as smooth curves in Figs. 1 and 2. The estimated absolute accuracy of K is ± 6%, while comparison of K values at different temperatures for a particular sample can be made to within ± 3% for $T < 2.2$ K and within ± 5% for $T > 2.2$ K.

We are interested in the phonon scattering produced by the added impurity atoms, not the phonon scattering occurring in the pure material due to boundaries and isotopes. However, in plots of $\ln(K)$ vs $\ln(T)$, such as in Fig. 1 and 2, the T^3 variation due to boundary scattering obscures the scattering produced by the added impurities, particularly at the lower concentrations. By plotting the ratio of the thermal conductivity of the doped sample (K_D) to the thermal conductivity of the equivalent "pure" sample (K_D), the effect of the added impurities is illustrated more clearly. K_P is calculated from Eqs. (A1) and (A2) with τ_{ep}^{-1} set equal to zero. The values for normal germanium found by Callaway,[18] i.e., $A_I = 2.57 \times 10^{-44}$ sec^3 and $B' = 2.77 \times 10^{-23}$ sec deg^{-3} were used for all calculations of K_p. For each sample, the value for the Casimir length L_c[19] (listed in Table I) was used along with $v_1 = 5.37 \times 10^5$ cm/sec and $v_2 = v_3 = 3.28 \times 10^5$ cm/sec, as calculated by Hasegawa[20] from the measured elastic constants of germanium.

For the pure n-type sample Ge-543 with 5.4×10^{13}

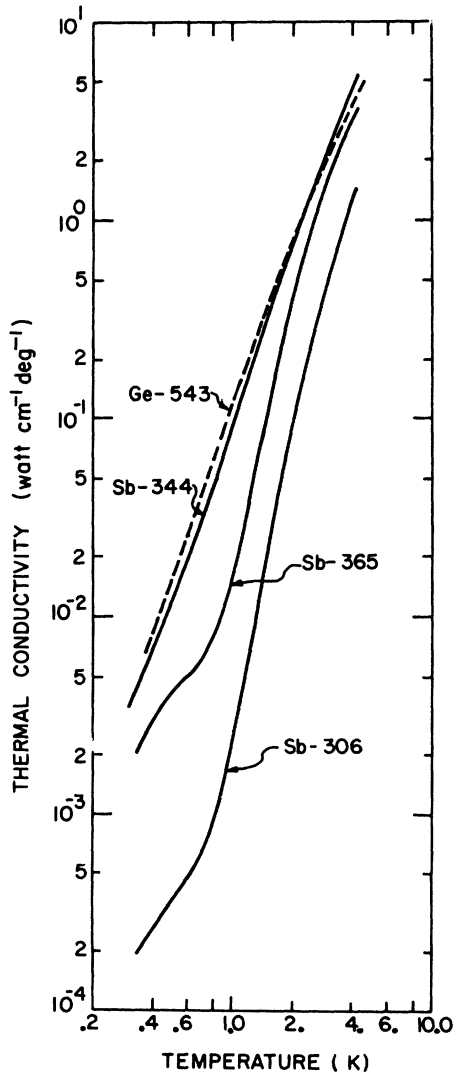

FIG. 1. Thermal conductivity of pure and Sb-doped germanium. Dopings are given in Table I.

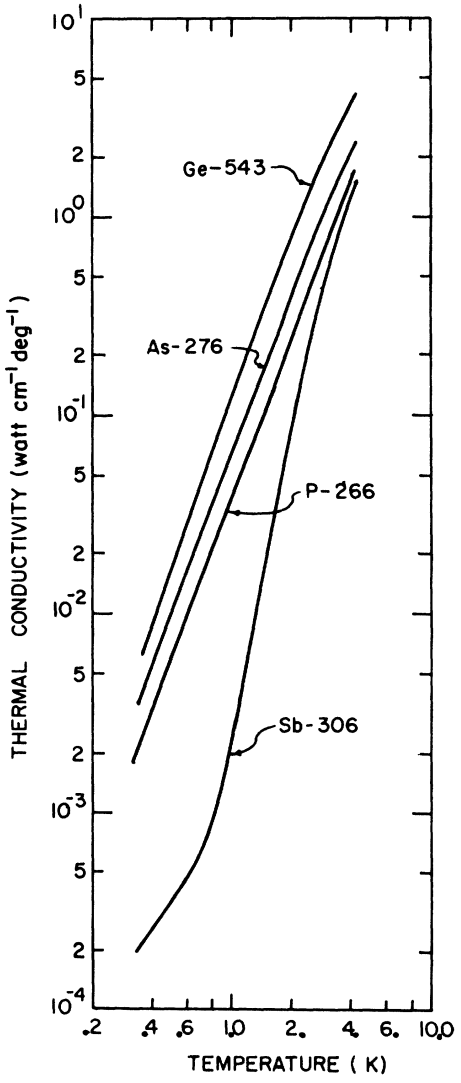

FIG. 2. Thermal conductivity of pure, As-, P-, and Sb-doped germanium. Dopings are given in Table I.

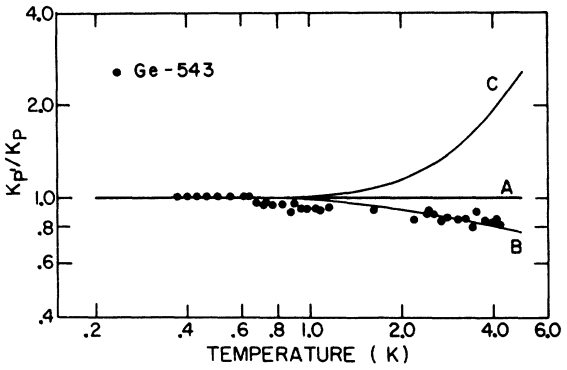

FIG. 3. Thermal-conductivity ratios $K_{P'}/K_P$ for measured values of pure Ge (circles) and values calculated with various scattering parameters (see text).

impurities per cm^3, the ratio K_D/K_p is replaced in Fig. 3 by the ratio $K_{p'}/K_p$, is indicating that the thermal conductivity of the pure sample ($K_{p'}$) is also calculated with τ_{ep}^{-1} in Eq. (A2) set equal to zero. Thus, $K_{p'}/K_p = 1$ (curve A) represents the pure material assuming diffuse boundary scattering ($L_c = 1.13A^{1/2}$ and Callaway's values for A_I and B'. Below 0.65 K, the measured thermal conductivity varies as T^3 and agrees within 1% of that calculated using Casimir's value for L_c. This also indicates that the relation between T^* and T given by Roberts *et al.*[13] for the paramagnetic salt (CMA) is correct down to at least 0.35 K. The only other measurement on pure germanium down to these low temperatures are those of Carruthers *et al.*[10] who measured two n-type samples with 10^{13} impurities per cm^3 and sand-blasted surfaces between 0.2 and 4.2 K in an adiabatic demagnetization apparatus. The experimental value found for one of their samples (Ge 2) was about 15% larger than that calculated from Casimir's formula. Unfortunately, it is unclear as to exactly what value they used for the velocity of sound, so that a quantitative comparison with their results cannot be made. Their other pure germanium sample (Ge 5) had a thermal conductivity that was smaller than Ge 2 by a factor of 2 in the T^3 boundary-scattering region, even though its calculated Casimir length was only 20% smaller.

Curve B in Fig. 3 is obtained using $A_I = 5.00 \times 10^{-44}$ sec^3 and $B' = 4.00 \times 10^{-23}$ sec/deg^3 in the calculation of $K_{p'}$. Toxen[21] found that these values gave the best fit to his thermal-conductivity measurements on a pure germanium sample from 2 to 50 K. The data for Ge-543 in Fig. 3 lie closer to the curve calculated from Toxen's value for A_I than to the curve corresponding to Callaway's value. Toxen pointed out, however, that his value of A_I was larger by a factor of 2 than that calculated on the basis of Klemens's theoretical expression (see Appendix A). Since Toxen obtained good agreement for a series of Ge-Si alloys, he attributed this large discrepancy in his "pure" sample either to a systematic error in the high-temperature data (15–50 K) for the sample, or to the presence of an unknown scattering process. We have therefore chosen to use Callaway's value for A_I and B' in all the calculated curves since these values give reasonable fits to the thermal conductivity of both normal and isotopically enriched germanium over the temperature range 3–100 K. As can be seen in Fig. 3, the difference between Callaway's and Toxen's values of A_I affects the calculated thermal-conductivity ratio by 20% at 4 K; however, below 2 K, where phonon scattering by bound donor electrons is important, the difference is insignificant. The contribution of three-phonon processes to the thermal conductivity is less than 1% below 4 K, so that uncertainty in the value of B' can be neglected.

The relative importance of scattering due to isotopes can be seen from curve C in Fig. 3. For curve C only boundary scattering was included in the calculation of $K_{p'}$. In comparison with curve A it can be seen that isotope scattering reduces the thermal conductivity by a factor of 2 at 4 K, but its importance becomes negligible below 1 K.

Figure 4 compares the data of sample Sb-365, containing 3.6×10^{15} Sb atoms per cm^3, with Keyes's model for the bound electron-phonon scattering process. Two separate measurements were made on this sample, indicated by the squares and triangles, in order to check on possible strains introduced by the method of attaching the thermometers or heater to the sample, or of mounting the sample to the cryostat. The data indicated by triangles were

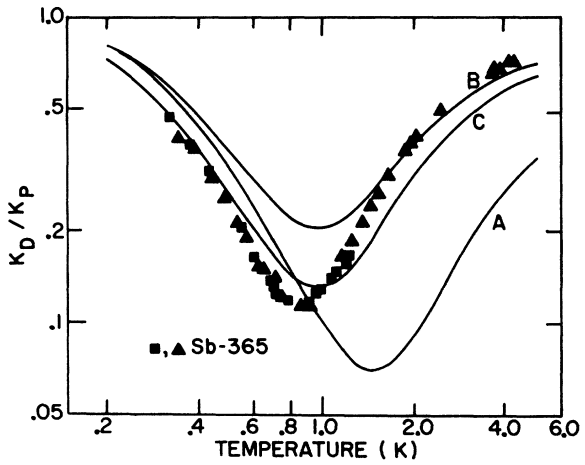

FIG. 4. Thermal-conductivity ratios between Sb-doped and pure samples: Points are measured values, smooth curves are calculated from Keyes's expression for scattering rate [Eq. (C1)] with values of parameters as listed in Table II.

taken with one end of the sample clamped to the He^3 pot and a heater clamped to the other end of the sample. The thermometers were glued to pure germanium slabs which were in turn soldered to the sample. The data indicated by squares were taken with each end of the sample soldered to thin tungsten slabs which were in turn soldered to the He^3 pot and to the heater, while the thermometers were glued directly to the sample. As the data indicate, very good agreement was obtained between the two separate measurements.

The curves indicated in Fig. 4 were obtained by including Keyes's expression for τ_{φ}^{-1} [(Eq. (C1)] in the calculation of K_D. Table II lists the values of the important parameters used in the calculation of K_D for the various curves in Figs. 4 – 9. For all calculations of K_D, the values used for v_s, L_c, A_I, and B' are the same as previously given for K_p. Also, for the Sb-doped samples the value of $4\Delta_c = 0.32$ meV will be used, as given by the infrared absorption measurements of Reuszer and Fisher.[22] There has been some dispute[23] as to the correct value of $4\Delta_c$ for Sb impurities in germanium. Recently however, Reuszer and Fisher studied the excitation spectra of Sb impurities under stress[24] and deduced the same value for $4\Delta_c$ (Sb) as they obtained previously from the zero-stress measurements.

Values for E_u, the shear deformation potential constant, and r_0, the effective radius of the ground-state donor wave function, can only be assigned within certain limits. E_u is a constant for which several measurements have been made, and the values found for germanium[25-30] lie between the limits of 16 and 19 eV. The lower limit of the parameter r_0 has been taken as r_H (the hydrogenic value listed in Table III, Appendix B), while the

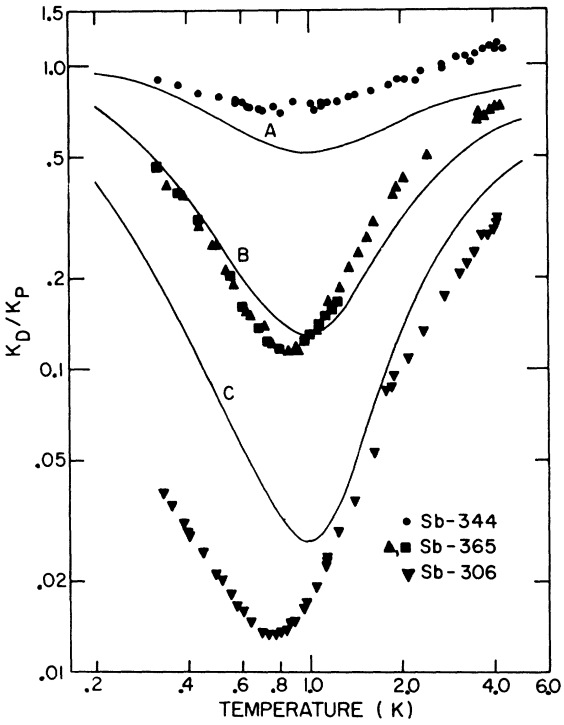

FIG. 5. Thermal-conductivity ratios between Sb-doped and pure samples: Points are measured values, smooth curves are calculated from Keyes's expression for scattering rate [Eq. (C1)] with values of parameters as listed in Table II.

TABLE II. Values of parameters used for theoretical curves.

Figure	Curve	N_{ex}(cm^{-3})	$4\Delta_c$(meV)	E_u(eV)	r_0(Å)	$B(T)$
4	A	3.6×10^{15}	0.32	16	44	···
	B	3.6×10^{15}	0.32	16	65	···
	C	3.6×10^{15}	0.32	19	65	···
5	A	3.4×10^{14}	0.32	19	65	···
	B	3.6×10^{15}	0.32	19	65	···
	C	3.0×10^{16}	0.32	19	65	···
6	A	3.6×10^{15}	0.32	16	44	1.0
	B	3.6×10^{15}	0.32	16	65	1.0
	C	3.6×10^{15}	0.32	19	44	1.0
	C′	3.6×10^{15}	0.32	19	44	Boltzmann factor
7	A	3.4×10^{14}	0.32	16	44	1.0
	B	3.6×10^{15}	0.32	16	44	1.0
	C	3.0×10^{16}	0.32	16	44	1.0
8	A	3.6×10^{15}	0.32	16	44	1.0
	B	3.0×10^{16}	0.32	16	44	1.0
	A′	3.6×10^{15}	0.32	16	44	···
	B′	3.0×10^{16}	0.32	16	44	···
9	A	3.7×10^{15}	2.83	16	35	1.0
	B	2.7×10^{16}	4.23	16	32	1.0
	C	2.6×10^{16}	2.83	16	35	1.0

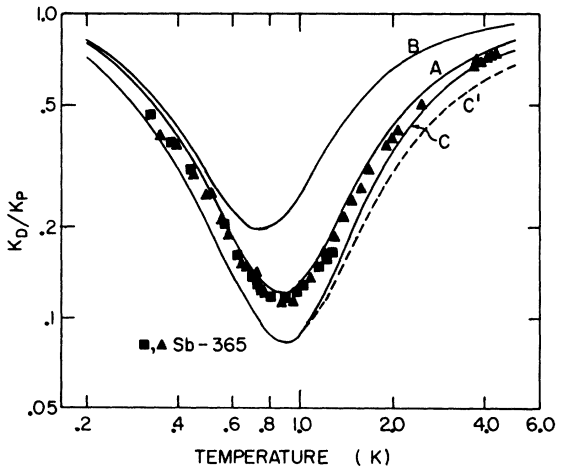

FIG. 6. Thermal-conductivity ratios between Sb-doped and pure samples: Points are measured values, smooth curves are calculated from the Griffin and Carruthers scattering rate [Eq. (C2)] with values of parameters as listed in Table II.

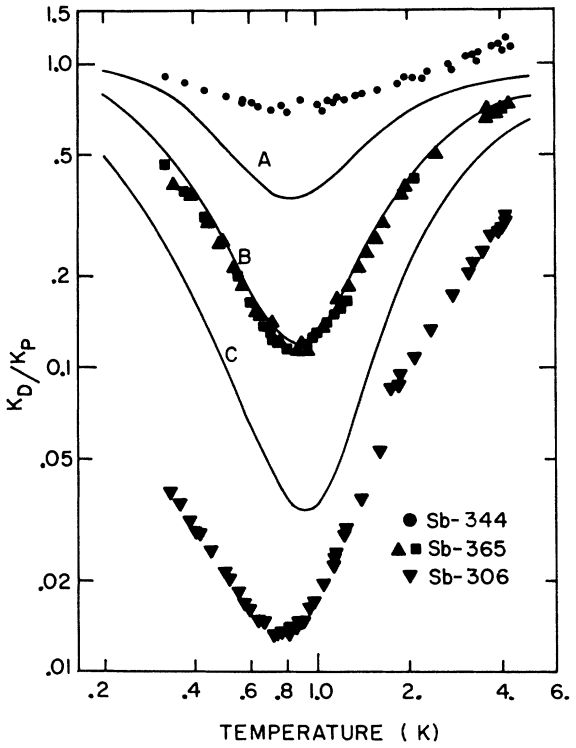

FIG. 7. Thermal-conductivity ratios between Sb-doped and pure samples: Points are measured values, smooth curves are calculated from the Griffin and Carruthers expression for scattering rate [Eq. (C2)], with values of parameters as listed in Table II.

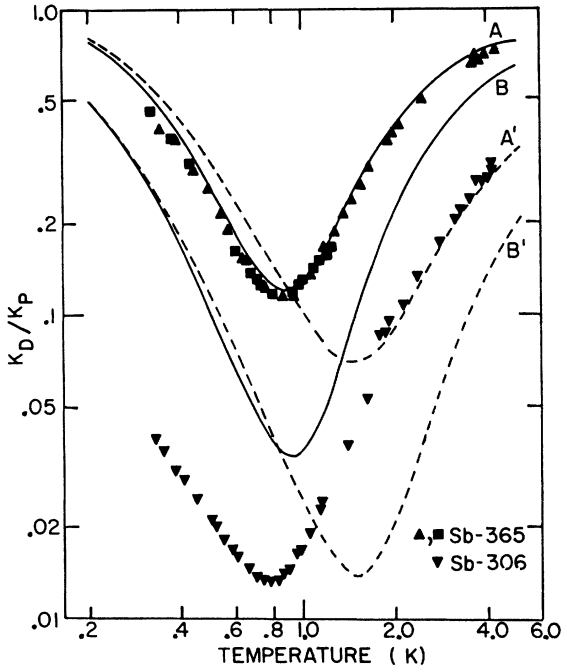

FIG. 8. Thermal-conductivity ratios between Sb-doped and pure samples: Points are measured values, smooth curves are calculated from Griffin and Carruthers expression for scattering rate [Eq. (C2)]—curves A, B; Keyes's expression [Eq. (C1)] is used for curves A′, B′. Parameter values for all curves are listed in Table II.

theoretical effective-mass value $r_{em} = 65$ Å has been used for the upper limit. Increasing the value of E_u from 16 to 19 eV increases the scattering equally on both sides of the region of maximum scattering. Increasing the value of r_0, on the other hand, shifts the region of maximum scattering to lower temperatures and reduces the amount of scattering. The curves in Fig 4 illustrate the scattering predicted by Keyes's model when different combinations of the limiting values of E_u and r_0 are used. Curve A results when $E_u = 16$ eV and $r_0 = 44$ Å is used in Keyes's expression. Changing r_0 to 65 Å gives curve B. The best fit to the data, curve C, is obtained with $E_u = 19$ eV and $r_0 = 65$ Å.

In Fig. 5, Keyes's model is compared with three samples containing different concentrations of Sb atoms. Curves A, B, and C are calculated using the values $E_u = 19$ eV and $r_0 = 65$ Å that gave the best fit to sample Sb-365. The calculated curves predict too much thermal resistance as compared to the data for the low-concentration sample Sb-334, but not enough thermal resistance for the higher-concentration sample Sb-306. Any change in E_u or r_0 to improve the agreement of theory and experiment for one sample would make the agreement worse for the other samples.

Above 2K, the measured thermal conductivity of sample Sb-344 with 3.4×10^{14} Sb atoms per cm^3 is higher than sample Ge-543 with only 5.4×10^{13} impurities per cm^3. It is difficult to account for this, unless at low concentrations the Sb atoms reduce the effect of an unknown scattering process occur-

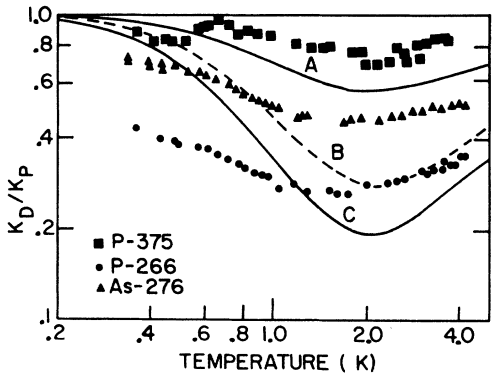

FIG. 9. Thermal-conductivity ratios between P- and As-doped and pure samples: Points are measured values, smooth curves are calculated with the Griffin and Carruthers expression for scattering rate [Eq. (C2)] with parameter values as listed in Table II.

TABLE III. Parameter values for shallow donors in germanium.

	Sb	P	As	Effective-mass theory
ϵ_i(meV)	10.19	12.76	14.04	9.2
$4\Delta_c$(meV)	0.32	2.83	4.23	0.0
$T_R(K) = 4\Delta_c/k$	3.71	32.8	49.1	...
r_0(Å)				
Hydrogenic ($r_H^{(1)}$)	44	35	32	49
Corr. effective mass (r_c)	44	39	37	46

ring in the "pure" germanium lattice.

Comparison of the Griffin-Carruthers expression for τ_{ep}^{-1} [Eq. (C2)] with measurements on sample Sb-365 is made in Fig. 6. Curve A, with $E_u = 16$ eV, $r_0 = 44$ Å, and $B(T) = 1$, gives excellent agreement between the experimental data and the theoretical curve. Changing r_0 to 65 Å gives curve B, while curve C is obtained using $E_u = 19$ eV, $r_0 = 44$ Å, and $B(T) = 1.0$. If it is assumed that the occupation probabilities of the singlet (B_S) and triplet state (B_T) are given by the usual Boltzmann factor, then $B_T/B_S = e^{-4\Delta_c/kT}$. Using this relation in the expression for $B(T)$ changes curve C to C′; similarly, this relation would somewhat improve the fit of curve A to the data.

In Fig. 7, the Griffin-Carruthers model is compared with three Sb-doped samples. Curves A, B, and C are calculated using the values $E_u = 16$ eV, $r_0 = 44$ Å and $B(T) = 1.0$ that gave the best fit to sample Sb-365. The calculated curves again predict too much thermal resistance for the low-concentration sample and not enough thermal resistance for the higher-concentration sample.

The importance of the resonance factor $R(\omega)$ [see Eq. (C2)] for the case of Sb donors can be seen in Fig. 8, where the curves obtained from both Keyes's and Griffin and Carruthers's expressions for τ_{ep}^{-1} are compared. All curves in Fig. 8 were calculated using $E_u = 16$ eV and $r_0 = 44$ Å. Curves A and B were calculated using Griffin and Carruthers's expression for τ_{ep}^{-1}, while Keyes's expression was used for curves A′ and B′. The presence of the resonance factor $R(\omega)$ increases the scattering slightly at lower temperatures and decreases it considerably at higher temperatures, thus shifting the region of maximum scattering to lower temperatures. In the case of sample Sb-365, curve A clearly gives a better fit to the data than curve A′. For sample Sb-306, neither curve B nor B′ gives a good fit to the data; but curve B gives a better fit than B′ in the sense that the temperature at which maximum scattering occurs is closer to that exhibited by the data. Also, curve B consistently predicts too little scattering at all temperatures while B′ predicts too much scattering at high temperatures and too little at low temperatures.

It might be hoped that the effect of the resonance factor $R(\omega)$ would indicate whether the resonance fluorescence mechanism proposed by Griffin and Carruthers gives better agreement between theory and experiment than Keyes's model, which does not take this effect into account. Unfortunately, as a comparison of Figs. 5 and 7 indicates, it is not clear, within the limits set for the parameters E_u and r_0, which approach gives a better fit to the data. However, as discussed in Appendix B, the electron spin-resonance measurements,[31] diamagnetic susceptibility measurements,[32] and ionization energy measurements (from which the corrected effective-mass value r_c is calculated),[33] indicate that r_0, at least for these phenomena, should be taken as approximately equal to the hydrogenic value r_H. This would mean that the additional scattering produced by the resonance fluorescence mechanism improves the agreement with the thermal-conductivity measurements.

Another feature of either Fig. 5 or 7 is that the measured scattering, particularly at the lower temperatures, increases faster with concentration that the calculated curves predict. The measurements on the P- and As-doped samples, shown in Fig. 9, also show this extra scattering at the lower temperatures. In particular, sample P-375 with 3.7×10^{15} atoms per cm^3 indicates a separate scattering peak at the lowest temperature.

Curves A and C, in Fig. 9, for the P samples were calculated from the Griffin and Carruthers expression for τ_{ep}^{-1} using $E_u = 16$ eV and $r_0 = r_H^{(1)} = 35$ Å. Curve B for the As-doped sample was calculated using $E_u = 16$ eV and $r_0 = r_H^{(1)} = 32$ Å. Keyes's expression for τ_{ep}^{-1} gives the same result within a few percent, since the resonance factor $R(\omega)$ is not effective due to the large $4\Delta_c$ for As or P donors (see Table III).

IV. DISCUSSION

At a concentration of 3×10^{16} atoms per cm^3, the three donor species all show more scattering at the lowest temperatures than predicted by either theoretical expression for τ_{ep}^{-1}. In addition, sample P-375 with 3.7×10^{15} P atoms per cm^3 exhibits what appears to be a separate resonance peak at the lowest temperatures. The question then arises as to whether this disagreement is due to various approximations introduced in the theoretical calculation or whether it is evidence for another scattering mechanism present at the lower temperatures. It is difficult to estimate how accurate one expects the theoretical calculation to be. However, at the lowest temperatures both Keyes's and Griffin-Carruthers's calculations agree, because in this

region the ω^4 dependence, typical of point-defect scattering, is dominant so that the strength of the scattering is determined essentially by the coefficient $[n_{ox}E_u^4/(4\Delta_c)^2]$, and any differences arising from different methods of averaging velocities and angular integrations are not important.

A consistent interpretation of the data for all the samples can be made by assuming that the disagreement between theory and experiment occurs not because of any approximations in the theory, but because of another mechanism that interacts strongly with phonons whose wavelengths are longer than those that interact with a single-bound donor electron. The disagreement between Griffin and Carruthers's expression for τ_{ep}^{-1} and experiment, as shown in Fig. 7, could then be explained in the following way: For the low-concentration sample Sb-334, with 3.4×10^{14} Sb atoms per cm^3, the additional scattering mechanism is weak and the Griffin-Carruthers expression for τ_{ep}^{-1} overestimates the amount of scattering due to the electron bound to a single donor; for sample Sb-365, the good agreement between theory and experiment is accidental, that is, the theory still overestimates the scattering due to the electron bound to a single donor, but now the additional scattering mechanism is strong enough to provide an apparent agreement between theory and experiment. At a concentration of 3×10^{16} Sb atoms per cm^3 (sample Sb-306) the additional scattering mechanism is so strong that the total amount of scattering is larger than can be accounted for by the theoretical calculation.

As can be seen in Fig. 9, for sample P-375, the theory again overestimates the amount of scattering due to the electron bound to a single donor and the actual magnitude of the scattering due to this process is weak enough to allow a separate resonance peak caused by the proposed additional scattering mechanism to be resolved. For the higher-concentration P- and As-doped samples the theory still overestimates the scattering at the higher temperature but underestimates it at lower temperatures where the additional scattering mechanism is important.

The proposed scattering mechanism then has the following properties: (a) It is strong in the low-temperature region where both the Keyes and the Griffin-Carruthers expressions for τ_{ep}^{-1} rapidly become ineffective; (b) its strength increases faster with concentration than predicted by either model of scattering due to an electron bound to a single donor; (c) it also appears to be species dependent; for example, contrast the large amount of excess scattering at the lower temperatures for Sb-306 with the smaller excess scattering of either samples P-266 or As-276, which have approximately the same impurity concentration.

The above properties suggest that the additional scattering arises from a defect involving more than one donor. Such a defect is important for impurity conduction[17,34–36] in the low-concentration range where charge transport occurs due to the phonon-assisted hopping of an electron between an ionized impurity pair (neutral donor + ionized donor) in the field of an ionized acceptor.[37–39] In his original article, Keyes[1] estimated that the phonon mean free path due to scattering by the hopping mechanism was never less than 1 cm in samples with concentrations of about 2×10^{16} donors per cm^3. Unfortunately, he did not give any details of how this estimate was calculated, except to mention that he used the electron-transition probabilities given by Miller and Abrahams[39] for this process. Recently, however, Takeyama[40] has pointed out that Miller and Abrahams's expression for the electron-transition probability should be larger by a factor of 4. Since the phonon mean free path varies inversely as the hopping rate of the electron, this would imply that the correct value for the phonon mean free path is of the order of 0.25 cm, which is one-half the mean free path due to boundary scattering, and therefore indicates that phonon scattering by this mechanism may be important. A detailed calculation of the phonon scattering produced by this process would be of interest.

In conclusion, the results of this investigation can be summarized as follows. Inclusion of the effect of resonance fluorescence scattering of phonons, as suggested by Griffin and Carruthers, in Keyes's model for scattering of phonons by the bound donor electron, improves the agreement between the theoretical and experimental values of the thermal conductivity for Sb-doped samples if the effective radius of the ground-state donor wave function is taken equal to that calculated, assuming a simple hydrogenic model of the donor impurity. The presence of additional scattering at the lower temperatures for the Sb-, As-, and P-doped samples may be evidence of an additional scattering mechanism, possibly that arising from the phonon-assisted hopping of the electron between donor impurities.

APPENDIX A: THERMAL-CONDUCTIVITY INTEGRAL

The usual expression for the thermal conductivity of a crystalline solid, assuming the single relaxation-time approximation and a Debye density of states $(\omega^2/2\pi^2 v_s^3)$, is given by

$$K(T)=\frac{k^4 T^3}{6\pi^2\hbar^3}\sum_{s=1}^{3}\frac{1}{v_s}\int_0^{\Theta_D/T}\frac{x^4 e^x}{(e^x-1)^2}\tau_s(x,T)dx, \tag{A1}$$

where $x=\hbar\omega/kT$, Θ_D is the Debye temperature, and the sum is over the three polarization modes.

A full discussion of the thermal conductivity of crystalline solids is given in the books by Peierls[41] and Ziman[42]; and in the review articles by Klemens,[43,44] Carruthers,[45] and Berman.[46] The particular case of the thermal conductivity of semiconductors is discussed in a book by Drabble and Goldsmid.[47]

In the temperature range of interest, the dominant scattering mechanisms are boundary scattering and neutral donor scattering. Isotope scattering and normal three-phonon processes scattering will also be included. The total relaxation time τ_s is found by combining reciprocal relaxation times of the different scattering mechanisms, as suggested by Klemens[43] and by Callaway,[18]

$$\tau_s^{-1} = \tau_{B,s}^{-1} + \tau_I^{-1} + \tau_N^{-1} + \tau_{ep,s}^{-1} , \tag{A2}$$

where $\tau_{B,s}^{-1}$, τ_I^{-1}, τ_N^{-1}, and $\tau_{ep,s}^{-1}$ represent scattering due to boundaries, isotopes, three-phonon processes, and neutral donors, respectively.

Casimir's[19] expression for boundary scattering will be modified in order to account for the difference in velocity of the longitudinal and transverse waves, that is, $\tau_{B,s}^{-1} = v_s/L_C$. The Casimir length $L_C = 1.13A^{1/2}$ defines an effective mean free path associated with a sample of cross-sectional area A, assuming diffuse boundary scattering.

The isotopic relaxation time $\tau_I^{-1} = [V_0\Gamma/(4\pi v^3)]\omega^4 = A_I\omega^4$, as given by Klemens,[43] will be used, where V_0 is the atomic volume, v is an average sound velocity, and Γ is a constant determined by the relative abundance of the isotopes and their masses. Substituting the values appropriate for germanium, $V_0 = 22.6\times10^{-24}$ cm^3, $\Gamma = 5.89\times10^{-4}$, and $v = 3.56\times10^5$ cm/sec, as calculated from the Debye temperature of germanium ($\Theta_D = 375$ K), gives a theoretical value for $A_I = 2.35\times10^{-44}$ sec^3. It should be noted that it would be more consistent to take the polarization dependence of the sound velocity into account when using τ_I^{-1} in the thermal-conductivity integral, as was done for boundary scattering. However, since in the temperature range of interest the isotopic contribution is small, the usual approximation of taking A_I to be the same for all three branches will be followed.

Callaway,[18] in his phenomenological development of an appropriate method of combining various scattering processes in the thermal-conductivity integral, suggested that scattering due to momentum conserving normal processes could be allowed for by including their relaxation time as part of the total relaxation time τ_s^{-1}. Using Herring's[48] suggested form for the relaxation time for low-frequency phonon-phonon scattering ($\tau_N^{-1} \propto \omega^j T^{5-j}$), Callaway was able to fit the thermal conductivity of normal and isotope-enriched germanium reasonably well over the range 2–100 K. Taking $\tau_s^{-1} = v/L_C + A_I\omega^4 + B'\omega^2 T^3$, where $j = 2$ (characteristic of longitudinal modes in a cubic crystal) is used in Herring's expression for τ_N^{-1}, he obtained the best fit with $A_I = 2.57\times10^{-44}$ sec^3 and $B' = 2.77\times10^{-23}$ sec deg^{-3}.

APPENDIX B: SHALLOW DONORS IN GERMANIUM

The group-V elements Sb, P, or As enter the germanium lattice substitutionally; four of the five valence electrons form covalent bonds with the neighboring germanium atoms, while the remaining electron is loosely bound by the reduced Coulomb potential due to the impurity ion of $V = \epsilon/\kappa r$, where κ is the static dielectric constant of the host lattice. The simple hydrogenic model[49,50] of the impurity leads to a set of reduced hydrogenic levels $\epsilon_n = R(m^*/m)(1/\kappa^2 n^2)$, and an orbital radius $r_H^{(n)} = a_0(m/m^*)\kappa n^2$, where n, the principal quantum number, is an integer, m^*/m is the effective-mass ratio, $R = 13.6$ eV is the Rydberg, and $a_0 = 0.53$ Å is the Bohr radius of the ground state of hydrogen. Substituting the values appropriate for germanium ($\kappa = 16$ and $m^*/m = 0.22$) results in a donor ionization energy $\epsilon_i = 0.012$ eV and a ground-state orbital radius $r_H^{(1)} = 39$ Å.

While the hydrogenic model predicts energy-level values that are in approximate agreement with experimental values, a more detailed theoretical treatment has been developed called the "effective-mass approximation"[33,51] that takes into account the band structure of the host lattice by replacing the spherical hydrogenlike wave functions of the simple model by four ellipsoidal wave functions, corresponding to the four conduction-band minima in Ge. Kohn's calculation gave the values $a = 65$ Å and $b = 23$ Å for the semimajor and semiminor axes of each ellipsoid, and an ionization energy of $\epsilon_{em} = 0.0092$ eV. Summing over the contributions from the four valleys results in an approximately spherical wave function with an effective radius $r_{em} = 65$ Å.

There is good agreement between the excited levels calculated from the effective-mass theory and those observed in infrared absorption by Reuszer and Fisher,[22] but not for the ground state. The effective-mass approximation predicts the same ionization energy for all group-V donors and a fourfold degenerate ground state; however, the actual ground state is shifted down and split into a singlet ground state and a triply degenerate state slightly above it. This splitting is species dependent and is referred to as the "chemical shift" or "valley-orbit splitting" and is denoted by $4\Delta_c$. Values of $4\Delta_c$, reported by Reuszer and Fisher, are given in Table III. Quantitatively, the breakdown in the effective-mass theory for the ground-state energy occurs because the s-like ground-state wave function has a finite amplitude in the region close to the donor ion where the assumption of a potential

of the form $V = e/\kappa r$ no longer is valid.

Kohn[33] corrected the effective-mass formulation by calculating the ellipsoidal wave functions corresponding to the observed ionization energies ϵ_i which are also given in Table III for the different impurities. These corrected wave functions give much better agreement between the theoretical value for $|\Psi(0)|^2$ and that observed by Wilson[31] in electron spin-resonance measurements of the hyperfine interaction of the donor electron and the donor neuclei. The corrected wave function for large values of r has an effective Bohr radius $r_c = \langle r_{em} \rangle (\epsilon_{em}/\epsilon_i)^{1/2}$, where $\langle r_{em} \rangle = (a^2 b)^{1/3} = 46$ Å represents an average over the ellipsoidal parameters of the effective-mass calculation. Values of r_c are also listed in Table III.

If the observed values for the donor ionization energy are used along with the expression given by the hydrogenic model for the effective Bohr radius ($r_H^{(1)} = a_0 R/\kappa\epsilon_i$), the values listed in Table III are obtained. Magnetic susceptibility measurements by Damon and Gerritsen[32] on As- and Sb-doped germanium with concentrations from 10^{16} to 10^{17} cm^{-3} indicated that the hydrogenic values $r_H^{(1)}$ gave better agreement for the orbital diamagnetism of weakly interacting donors than did the effective-mass value of 65 Å. Wilson[31] has estimated an average radius for the donor wave function from measurements of the linewidths of spin-resonance lines due to hyperfine interactions of the donor electron with the Ge^{73} isotope. He obtained values of 32 Å for phosphorus and 30 Å for arsenic.

APPENDIX C: THEORETICAL MODELS FOR ELECTRON-PHONON SCATTERING

In order to explain the thermal-conductivity measurements of Goff and Pearlman, Keyes[1] proposed a model in which the phonon scattering arises from the large effect of strain on the energy of the bound donor electrons leading to virtual transitions between the singlet and triplet states. The electronic energy states have a quadratic dependence on the strain produced by the phonon, resulting in scattering of the point-defect type ($\tau^{-1} \propto \omega^4$). A further dependence on the phonon frequency (ω) arises when the phonon wavelength becomes shorter than the diameter of the electronic orbit ($2r_0$), causing the average strain experienced by the electron to approach zero, so that the phonon scattering rapidly decreases as the phonon frequency rises past $\omega \sim v_s/r_0$. This results in a scattering rate which Keyes expresses in the form

$$\tau_{ep}^{-1}(\omega, s)^K = M(\omega) V(v_s) G(\omega, s), \tag{C1}$$

with

$$M(\omega) = \frac{1}{3^4 \pi \rho^2} \frac{n_{ex} E_u^4 D_s}{(4\Delta_c)^2} \omega^4 ,$$

$$V(v_s) = \tfrac{2}{5} \left(\tfrac{2}{3} 1/v_1^7 + 1/v_2^7\right) ,$$

and the cut-off factor $G(\omega, s)$ given by

$$G(\omega, s) = [1 + (r_0 \omega / 2 v_s)^2]^{-8} .$$

In Eq. (C1), s is the polarization index for the acoustical branches ($s = 1, 2, 3$), v_s is the velocity of sound, ρ is the density, n_{ex} is the concentration of neutral donors, E_u is the shear deformation potential constant,[52] and D_s is an anisotropy factor with the values $D_1 = \frac{4}{5}$, $D_2 = D_3 = \frac{3}{5}$.

Keyes's expression for the inverse relaxation time is small at low frequencies because of the ω^4 dependence, reaches a maximum at $\omega \sim v_s/r_0$, then rapidly decreases due to the cut-off factor $G(\omega, s)$. It is species dependent through its dependence on $4\Delta_c$ and r_0.

In a more detailed calculation, Griffin and Carruthers[2] argued that, whereas Keyes treated the donor electron as moving in the static strain field created by the phonons, the electron actually adjusts to the phonon perturbation with a characteristic frequency $4\Delta_c/h$ which lies in the range of frequencies important for heat conduction. They therefore treated the problem in analogy with the resonance fluorescence scattering of photons. Using this approach, Griffin and Carruthers obtained the following expression for the inverse relaxation time:

$$\tau_{ep}^{-1}(\omega, s)^{GC} = M'(\omega) R(\omega) W(\omega, v_s, s) B(T) , \tag{C2}$$

with

$$M'(\omega) = \frac{1}{3^4 \pi \rho^2} \frac{n_{ex} E_u^4 H_s}{(4\Delta_c)^2} \omega^4 ,$$

$$R(\omega) = (4\Delta_c)^4 / [(\hbar\omega)^2 - (4\Delta_c)^2]^2 ,$$

$$W(\omega, v_s, s) = \frac{1}{P_s v_s^2} \left(\frac{1}{P_1 v_1^5} + \frac{3}{2 P_2 v_2^5} \right) ,$$

$$B(T) = \{ B_s(T) + B_T(T) [2 + (\hbar\omega/4\Delta_c)^2] \} .$$

In Eq. (C2), H_s is an anisotropy factor with the values $H_1 = \frac{48}{225}$, $H_2 = \frac{32}{225}$, and $H_3 = \frac{40}{225}$; P_s is related to the cut-off factor $G(\omega, s)$ in Keyes's expression by the relation $P_s^2 = 1/G(\omega, s)$; and $B_s(T)$ and $B_T(T)$ are the occupation probabilities for the singlet and triplet states. If all electrons are assumed to be in the ground state, then $B_s(T) = 1.0$ and $B_T(T) = 0.0$.

Comparing the two expressions for the relaxation time, the major difference, aside from those arising from different methods of averaging velocities and angular integrations, is the presence of the "true resonance factor" $R(\omega)$ in the Griffin-Carrathers expression for τ_{ep}^{-1}. Note in the limit of $\hbar\omega \ll 4\Delta_c$ that $R(\omega)$ approaches 1.

*Research supported by the Advanced Research Projects Agency.

†Present address: Naval Ship Research and Development Center, Annapolis, Md.

[1]R. W. Keyes, Phys. Rev. 122, 1171 (1961).

[2]A. Griffin and P. Carruthers, Phys. Rev. 131, 1976 (1963).

[3]M. G. Holland, in *Semiconductors and Semimetals*, edited by R. K. Willardson and A. C. Beer (Academic, New York, 1966), Vol. 2, p. 3.

[4]S. S. Devlin, in *Physics and Chemistry of II-VI Compounds*, edited by M. Aven and J. S. Prener (North-Holland, Amsterdam, 1967), Chap. 11, p. 575.

[5]P. D. Maycock, Solid-State Electron. 10, 161 (1967).

[6]J. F. Goff and N. Pearlman, in *Proceedings of the Seventh International Conference on Low-Temperature Physics*, edited by G. M. Graham and A. C. Hollis Hallett (University of Toronto Press, Toronto, 1961), pp. 284–288.

[7]J. F. Goff and N. Pearlman, Phys. Rev. 140, A2151 (1965).

[8]M. P. Mathur, Phys. Rev. 180, 833 (1969).

[9]J. A. Carruthers, T. H. Geballe, H. M. Rosenberg, and J. M. Ziman, Proc. Roy. Soc. (London) 238A, 502 (1957).

[10]J. A. Carruthers, J. F. Cochran, and K. Mendelssohn, Cryogenics 2, 1 (1962).

[11]B. L. Bird, Ph. D. thesis (Purdue University, 1968) (unpublished).

[12]H. Montgomery, Cryogenics 5, 229 (1965).

[13]T. R. Roberts, S. G. Sydoriak, and R. H. Sherman, in *Temperature, Its Measurement and Control in Science and Industry*, edited by C. M. Herzfeld (Reinhold, New York, 1962), Vol. 3, part 1, pp. 75–87.

[14]D. E. Moody and P. Rhodes, Cryogenics 3, 77 (1963).

[15]C. Herring, Bell System Tech. J. 34, 237 (1955).

[16]R. A. Smith, *Semiconductors* (Cambridge U.P., London, 1959), p. 118.

[17]H. Fritzsche, J. Phys. Chem. Solids 6, 69 (1958).

[18]J. Callaway, Phys. Rev. 113, 1046 (1959).

[19]H. B. G. Casimir, Physica 5, 495 (1938).

[20]H. Hasegawa, Phys. Rev. 118, 1513 (1960).

[21]A. M. Toxen, Phys. Rev. 122, 450 (1961).

[22]J. H. Reuszer and P. Fisher, Phys. Rev. 135, A1125 (1964).

[23]R. E. Pontinen and T. M. Sanders, Jr., Phys. Rev. 152, 850 (1966).

[24]J. H. Reuszer and P. Fisher, Phys. Rev. 165, 909 (1968).

[25]J. R. Drabble and J. Fendley, J. Phys. Chem. Solids 28, 669 (1967).

[26]L. J. Bruner and R. W. Keyes, Phys. Rev. Letters 7, 55 (1961).

[27]B. Tell and G. Weinriech, Phys. Rev. 143, 584 (1966).

[28]S. Riskaer, Phys. Rev. 152, 845 (1966).

[29]H. Fritzsche, Phys. Rev. 115, 336 (1959).

[30]See Ref. 22, p. A1132.

[31]D. K. Wilson, Phys. Rev. 134, A265 (1964).

[32]D. H. Damon and A. N. Gerritsen, Phys. Rev. 127, 405 (1962).

[33]W. Kohn, in *Advances in Solid State Physics*, edited by F. Seitz and D. Turnbull (Academic, New York, 1957), Vol. 5, pp. 258–321.

[34]C. S. Hung and J. R. Gliessman, Phys. Rev. 79, 726 (1950).

[35]N. F. Mott and W. D. Twose, in *Advances in Physics*, edited by N. F. Mott (Taylor and Francis, London, 1961), Vol. 10, p. 107.

[36]E. A. Davis and W. Dale Compton, Phys. Rev. 140, A2183 (1965).

[37]N. F. Mott, Can. J. Phys. 34, 1356 (1956).

[38]E. M. Conwell, Phys. Rev. 103, 51 (1956).

[39]A. Miller and E. Abrahams, Phys. Rev. 120, 745 (1960).

[40]K. Takeyama, J. Phys. Soc. Japan 23, 1013 (1967).

[41]R. E. Peierls, *Quantum Theory of Solids* (Oxford U.P., London, 1955).

[42]J. M. Ziman, *Electrons and Phonons* (Oxford U.P., London, 1960).

[43]P. G. Klemens, in *Advances in Solid State Physics*, edited by F. Seitz and D. Turnbull (Academic, New York, 1958), Vol. 7, pp. 1—99.

[44]P. G. Klemens, in *Encyclopedia of Physics*, edited by S. Flügge (Springer-Verlag, Berlin, 1956), Vol. 14, pp. 198–281.

[45]P. Carruthers, Rev. Mod. Phys. 33, 92 (1961).

[46]R. Berman, Cryogenics 5, 297 (1965).

[47]J. R. Drabble and H. J. Goldsmid, *Thermal Conduction in Semiconductors* (Pergamon, Oxford, England, 1961).

[48]C. Herring, Phys. Rev. 95, 954 (1954).

[49]N. F. Mott and R. W. Gurney, *Electronic Processes in Ionic Crystals* (Oxford U.P., London, 1940).

[50]H. A. Bethe, MIT Radiation Laboratory Report No. 43-12, 1942 (unpublished).

[51]W. Kohn and J. M. Luttinger, Phys. Rev. 97, 1721 (1955); 98, 915 (1955).

[52]C. Herring and E. Vogt, Phys. Rev. 101, 944 (1956).